ARTICLES
https://doi.org/10.1038/s41560-021-00920-8
nature energy

Check for updates

Tailored catalyst microenvironments for CO_2 electroreduction to multicarbon products on copper using bilayer ionomer coatings

Chanyeon Kim[1,2,3], Justin C. Bui[1,2,3], Xiaoyan Luo[4], Jason K. Cooper[2,3], Ahmet Kusoglu[4], Adam Z. Weber[2,4] and Alexis T. Bell[1,2,3]✉

Electrochemical carbon dioxide reduction (CO_2R) provides a promising pathway for sustainable generation of fuels and chemicals. Copper (Cu) electrocatalysts catalyse CO_2R to valuable multicarbon (C_{2+}) products, but their selectivity depends on the local microenvironment near the catalyst surface. Here we systematically explore and optimize this microenvironment using bilayer cation- and anion-conducting ionomer coatings to control the local pH (via Donnan exclusion) and CO_2/H_2O ratio (via ionomer properties), respectively. When this tailored microenvironment is coupled with pulsed electrolysis, further enhancements in the local ratio of CO_2/H_2O and pH are achieved, leading to selective C_{2+} production, which increases by 250% (with 90% Faradaic efficiency and only 4% H_2) compared with static electrolysis over bare Cu. These results underscore the importance of tailoring the catalyst microenvironment as a means of improving overall performance in electrochemical syntheses.

Electrochemical conversion of H_2O and CO_2 using electricity from renewable sources (for example, wind and solar) provides a sustainable path for converting CO_2 into value-added chemicals and fuels. The most promising catalyst for CO_2 reduction (CO_2R) is copper (Cu), since it can produce multicarbon products (C_{2+} products), such as C_2H_4, C_2H_5OH and C_3H_7OH[1–3], rather than those containing only one carbon atom (C_1 products), such as HCOOH, CO and CH_4, or H_2. Of these products, those containing two or more carbon atoms are the most desirable because they can be readily converted to value-added chemicals and liquid fuels by conventional thermocatalytic processes[1–3]. The challenge to achieving this goal is identifying the means of increasing the concentration of CO_2 near the catalyst surface, reducing the formation of C_1 products relative to C_{2+} products and minimizing the conversion of H_2O, the electrolyte solvent, to H_2.

Both the Cu surface structure and the microenvironment near its surface influence the activity and selectivity of Cu for C_{2+} product formation. Rough Cu surfaces, produced by reconstruction of smooth surfaces or reduction of copper oxide or copper nitride, contain low coordination sites that are particularly active and selective for C_{2+} product formation[4–6]. The selectivity for C_{2+} products is further enhanced by operating at high electrolyte pH because this suppresses the formation of H_2, HCOOH, CO and CH_4 (refs. [7–9]). The choice of electrolyte cation also affects product selectivity. Hydrated Cs^+ cations, which have a smaller radius than hydrated Li^+ cations, create a stronger electrostatic field in the Helmholtz double layer, which in turn stabilizes the adsorption of CO_2 and C_{2+} intermediates, thereby enhancing the formation of C_{2+} products[10,11]. While high pH enhances C_{2+} product selectivity, it also leads to a substantial reduction in CO_2 concentration near the Cu surface due to formation of HCO_3^- and CO_3^{2-} via reaction of CO_2 with OH^- anions[12–14]. This effect limits the overall reaction rate, although it can be offset by carrying out CO_2R by pulsed, rather than static, electrolysis[7,15,16], because pulsing enables repeated access to transient conditions of high CO_2 concentration and high pH at the cathode surface, which are inaccessible in static electrolysis[7].

Recent studies have shown that the activity and selectivity of Cu for CO_2R can be modified further by introducing organic compounds on the surface of Cu[17–20]. These studies ascribe the improved selectivity to the increased hydrophobicity and/or CO_2 affinity of the organic layer, thereby enhancing the CO_2/H_2O ratio at the catalyst surface. Ion-conducting polymers (ionomers) can also modify the local concentrations of CO_2, H_2O, OH^- and H^+ because their backbone chains containing -CH_2- or -CF_2- induce hydrophobicity, and the charged moieties at the ends of the side chains modulate ion transport[20–23]. However, the impact of ionomers on CO_2R is poorly understood; so far, most studies have been empirical and have given inconsistent explanations for how ionomer films affect CO_2R. Therefore, it is important to develop a systematic understanding of how ionomer layers impact CO_2R by varying properties such as background charge, counterions and ion-exchange capacity. Such knowledge enables tailoring of the chemical microenvironment near a Cu catalyst for optimal C_{2+} product formation.

Here, we demonstrate that ionomer layers can be used to create favourable microenvironments for selective C_{2+} production on Cu. To elucidate fully the effects of ionomers on the local Cu catalyst microenvironment, we combine systematic investigations of CO_2R on Cu covered by different ionomer layers with a determination of the structure–property relationships of these ionomer films. The improved understanding thus gained, along with previous knowledge of pulsed electrolysis, is used to further enhance CO_2R activity and C_{2+} selectivity.

Properties of the ionomer under CO_2R-related environments

To develop a picture of how ionomer layers influence the ionomer/Cu system, it is useful to first review what is known about the

[1]Department of Chemical and Biomolecular Engineering, University of California, Berkeley, CA, USA. [2]Liquid Sunlight Alliance, Lawrence Berkeley National Laboratory, Berkeley, CA, USA. [3]Chemical Sciences Division, Lawrence Berkeley National Laboratory, Berkeley, CA, USA. [4]Energy Technologies Area, Lawrence Berkeley National Laboratory, Berkeley, CA, USA. ✉e-mail: alexbell@berkeley.edu

Table 1 | Thermodynamic and transport properties of aqueous electrolyte, Nafion and Sustainion

		Aqueous solution	Nafion	Sustainion
Water concentration (M)	Reported for bulk ionomer membrane	55.6	22.1 (H^+ exchanged)[43] 4.8 (Cs^+ exchanged)[43]	48.9 (OH^- exchanged)[44]
	Measured for thin film on Cu		18.7 (H^+ exchanged) 4.4 (Cs^+ exchanged)	24.9 (OH^- exchanged) 19.7 (HCO_3^- exchanged)
Reported CO_2 solubility for bulk ionomer membrane (mM)		34	36.1 (ref. [45])	<703 (ref. [24])[a]
Mole CO_2/H_2O (a.u., $\times10^{-4}$)		6.1	82.0 (Cs^+ exchanged)	<356.9 (HCO_3^- exchanged)
CO_2 permeability (10^{-16} mol cm^{-1} s^{-1} Pa^{-1})		64.94 (ref. [46])	8.70 (ref. [45])	<2.51 (ref. [24])[a]
Ionic conductivity (mS cm^{-1})		56.54[b]	70.1–200 (H^+ exchanged)[43,47] 1.1–20 (Cs^+ exchanged)[43,47]	64 (OH^- exchanged)[48] 24 (HCO_3^- exchanged)[48]

[a]Values taken from the literature for imidazolium-based anion-exchange membrane. [b]Value is for 0.1 M $CsHCO_3$ electrolyte.

properties of Nafion (a perfluorosulfonic acid, cation-conducting ionomer) and Sustainion (a polystyrene vinylbenzyl methylimidazolium, anion-conducting ionomer) in the $CsHCO_3$ bulk electrolyte used for CO_2R.

Table 1 summarizes the water concentration, CO_2 solubility, CO_2/H_2O equilibrium ratio at 1 bar CO_2 pressure and room temperature, CO_2 permeability, and ion conductivity, in aqueous solution as well as in Nafion and Sustainion membranes. The reported concentration of H_2O is about 12 times lower in the Cs^+-exchanged Nafion than in 0.1 M $CsHCO_3$ solution, but for Sustainion it is only 1.1 times lower. To determine the applicability of these trends to aqueous CO_2R on a Cu catalyst, water concentration was measured on thin ionomer films (<40 nm) deposited on Cu (Supplementary Fig. 1). These measurements demonstrated agreement with the water concentration measured for free-standing bulk membranes exchanged with the same counterions. The reported solubility of CO_2 in Nafion and aqueous $CsHCO_3$ are nearly identical, but the CO_2 solubility in Sustainion is a factor of 20 higher due to the presence of imidazolium groups with high CO_2 affinity[24]. These measurements suggest that under the conditions used for CO_2R, the ratio of CO_2/H_2O would be 13-fold higher in Cs^+-exchanged Nafion thin film compared to aqueous $CsHCO_3$, and about 58-fold higher in the HCO_3^--exchanged Sustainion. The permeability of CO_2 is highest for aqueous $CsHCO_3$ and decreases by a factor of nearly 7 and 26 for Nafion and Sustainion, respectively. The ion conductivity of the major charge carrier in Cs^+-exchanged Nafion and HCO_3^--exchanged Sustainion is lower than that for Cs^+ and HCO_3^- in the electrolyte itself. We note, for comparison, that H^+-exchanged Nafion and OH^--exchanged Sustainion have slightly higher ion conductivities than the bulk electrolyte.

An important issue is whether the ionomer film limits the rate of electrolysis due to either CO_2 mass transport or ionic transport limitations. Calculations demonstrate that neither phenomenon is limiting at a total current density (TCD) of 10 mA cm^{-2} (Supplementary Notes 1 and 2).

The effect of the ionomer-coated Cu on CO_2R

To validate the proposed microenvironment design, ionomer layers of Nafion and Sustainion were drop-cast onto a Cu film. The optimum loading for CO_2R was 6 μg cm^{-2} for each ionomer (Supplementary Note 3 and Supplementary Fig. 2). Nafion-coated Cu (Naf1100/Cu, Nafion with 1,100 g mol$_{eq}^{-1}$ equivalent weight (EW)) and Sustainion-coated Cu (Sus/Cu) were characterized by a scanning electron microscope equipped with an energy-dispersive X-ray spectrometer (Fig. 1a,b). The thickness of the Cu film deposited on a polytetrafluoroethylene (PTFE) membrane used to support the catalyst was around 400 nm, and that of the Nafion layer on Cu was up to 30 nm, on the basis of the F elemental line scan. Similarly, using the Cl elemental line scan, the thickness of the Sustainion layer on the as-prepared sample was estimated to be 40 nm. To identify the effects of the ionomer layers on the activity and selectivity of Cu for CO_2R, the catalytic performances of Naf1100/Cu and Sus/Cu were measured and compared to that of bare Cu at applied potentials from −0.8 to −1.15 V versus the reversible hydrogen electrode (RHE) (Fig. 2a–d and Supplementary Fig. 3). The Nafion layer produced no noticeable change in the TCD relative to that of bare Cu, but substantial changes were observed in the product distribution. For example, at −1.15 V versus RHE, the Faradaic efficiency (FE) for H_2 was suppressed from 20 to 9%, and the FE for C_{2+} products was enhanced from 60 to 70%. In the case of Sustainion, at all potentials tested there was only a marginal change in the product distribution but a noticeable increase in the TCD with increasing potential compared to bare Cu. As shown in Supplementary Fig. 4, the FE values for H_2, C_1 products and C_{2+} products exhibited very similar potential-dependent behaviour to those observed for bare Cu.

Since the water concentration in contact with the Cu surface decreases in the order of bare Cu > Sus/Cu > Naf1100/Cu (Fig. 2e), the partial current density for CO_2R in the presence of ionomer layers behaves as expected, on the basis of the CO_2/H_2O ratio corresponding to the local CO_2 concentration given in Fig. 2f. In addition, when identical experiments were performed using Nafion with a lower EW (850 g mol$_{eq}^{-1}$, denoted as Naf850/Cu) (Fig. 2d), the C_{2+} selectivity increased further, while the TCD decreased only slightly. As shown in Fig. 2e, Naf850/Cu has a higher water concentration than Naf1100/Cu because of its higher concentration of hydrophilic sulfonate groups. Thus, while a slight decrease in the TCD for Naf850/Cu can be attributed to a slight decrease in the local CO_2/H_2O ratio compared with that for Naf1100/Cu, the enhanced C_{2+} selectivity is counterintuitive and cannot be attributed solely to the higher CO_2/H_2O ratio.

The effect of electrolyte cation

To evaluate the effect of electrolyte cation on CO_2R in the presence of an ionomer layer, CO_2R was conducted with 0.1 M of $LiHCO_3$, as shown in Fig. 3a–d and Supplementary Fig. 5. All of the tested Cu catalysts exhibited much lower TCD and selectivity for CO_2R, in good agreement with previous reports regarding the effect of alkali cations on CO_2R on Cu[10]. Nonetheless, the qualitative impact of depositing Sustainion or Nafion ionomer layers on Cu is consistent regardless of cation identity. As shown in Fig. 3e, Li^+-exchanged Naf1100/Cu and Naf850/Cu exhibited higher water concentrations compared to the corresponding Cs^+-exchanged materials, but these concentrations were still considerably lower than for bare Cu. The local CO_2/H_2O ratio exhibited a similar trend to that observed with Cs^+, the CO_2/H_2O ratio increasing in the order bare Cu < Naf850/Cu < Naf1100/Cu < Sus/Cu. Thus, the extent of increase in CO_2R activity on changing the cation identity is probably associated

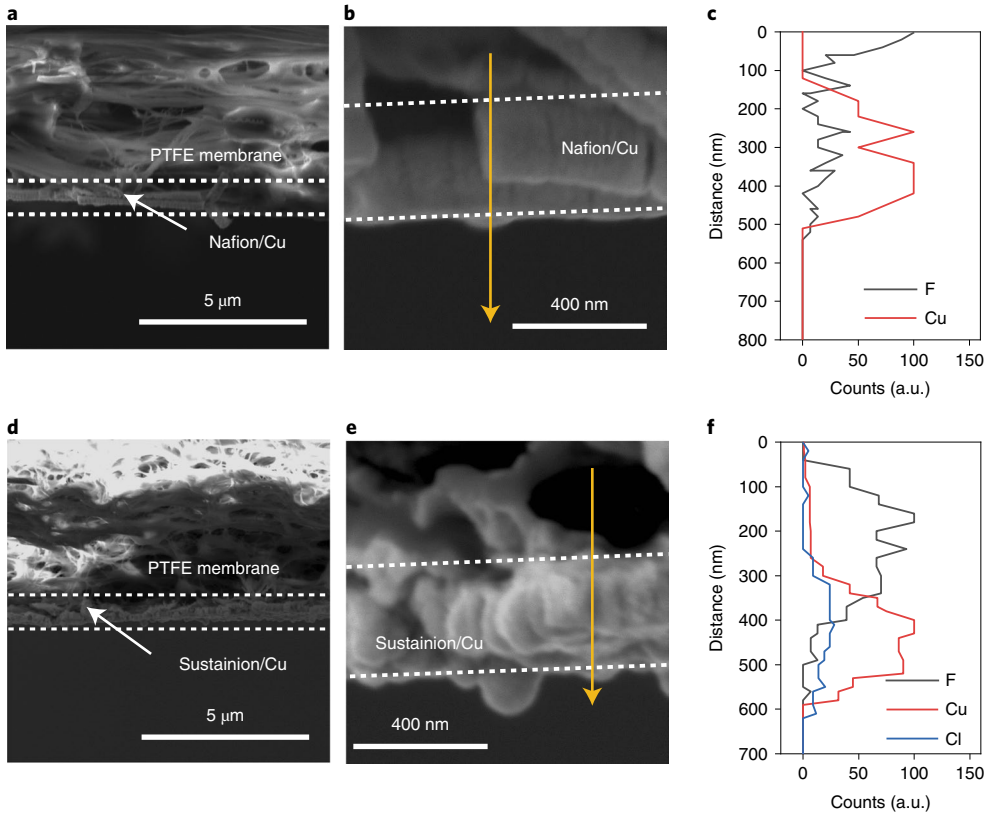

Fig. 1 | Morphological and compositional analysis on ionomer-coated Cu. a–f, SEM images (**a**,**b**,**d**,**e**) and elemental line scans (**c**,**f**) of Naf1100/Cu (**a**–**c**) and Sus/Cu (**d**–**f**).

with the local CO_2/H_2O ratio, but it cannot explain the enhanced C_{2+} selectivity for Naf1100/Cu and the further enhancement for Naf850/Cu.

The most compelling explanation for the enhanced C_{2+} selectivity can be derived by considering Donnan exclusion at the interface between the Cu and the ionomer[25]. A key difference between Sustainion and Nafion is the background charge of the polymers, which are positive and negative, respectively. Thus, the negative background charge in Nafion causes exclusion of anions and accumulation of CO_2R-generated OH^- at the Cu surface (that is, higher local pH). This hypothesis agrees with previous work, which demonstrated that enhancements in selectivity for C_{2+} over C_1 products and H_2 are primarily driven by pH, and that the ratio of CO_2/H_2O is only responsible for enhancing CO_2R current density[7]. This phenomenon was also noted for CO_2R to formate versus CO on Ag with varying Nafion loadings, where higher Nafion loadings were hypothesized to increase the local pH[26]. Similar reasoning also helps to explain the results observed for CO_2R with Sus/Cu. The TCD for CO_2R is increased due to the increased CO_2/H_2O ratio, but because OH^- transport is uninhibited in Sustainion, the pH in the Sus/Cu microenvironment remains similar to that in the pure aqueous environment; the product distribution is unchanged. Lastly, this interpretation also explains the observed C_{2+} selectivity enhancement when switching from Naf1100 to Naf850. Despite the increased water content of Naf850/Cu, because Naf850 possesses a higher background charge density, it exhibits stronger Donnan exclusion, which enables a greater amount of OH^- build-up, resulting in increased C_{2+} selectivity.

Origin of the enhanced rate of CO_2R on ionomer-coated Cu

Our hypothesis about the role of the ionomer layer in CO_2R is that it modulates the microenvironment (local CO_2/H_2O ratio and pH) near the Cu catalyst. Therefore, it is important to confirm that the observed selectivity enhancements are indeed due to changes in the chemical microenvironment and not due to an intrinsic change in the Cu surface. To address this question, we investigated the effect of different ionomer-layer stacks (that is, bilayer thin films) on Cu CO_2R performance, as shown in Fig. 4a and Supplementary Fig. 6. We found that the ionomer coating does not noticeably affect the roughness of the Cu and that the electrochemical surface areas for bare Cu and all ionomer-coated Cu samples are very similar, as shown in Supplementary Fig. 7. When a Sustainion layer was deposited on top of Naf850/Cu (Sus/Naf850/Cu), the TCD increased relative to that for Naf850/Cu, but no noticeable change in product distribution occurred. Interestingly, the addition of a Nafion layer on top of Sus/Cu (Naf850/Sus/Cu) resulted in increased C_{2+} production, from 61 to 80% FE, and decreased H_2 production, from 18 to 5% FE, with a concomitant TCD above that for Naf850/Cu. Thus, these differences result in the increase of all the partial current densities compared to Naf850/Cu in the case of Sus/Naf850/Cu, while in the case of Naf850/Sus/Cu, a selective increase of partial current density for C_{2+} products in comparison with Sus/Cu results (Supplementary Fig. 8).

Moreover, the observed effects of stacking ionomers are consistent with not only identical experiments using Naf1100 (Supplementary Fig. 9), but also experiments using a flat Cu surface prepared by sputtering a 400-nm Cu film onto a Si wafer, as shown in Supplementary Fig. 10a. The configuration of the 'bilayer' coating for this system was confirmed by X-ray photoemission spectroscopy analysis (Supplementary Fig. 10b–d). These observations clearly indicate that the individual effects of each ionomer layer are apparent regardless of their stacking order, thereby suggesting that the role of the ionomer in improving catalytic CO_2R performance

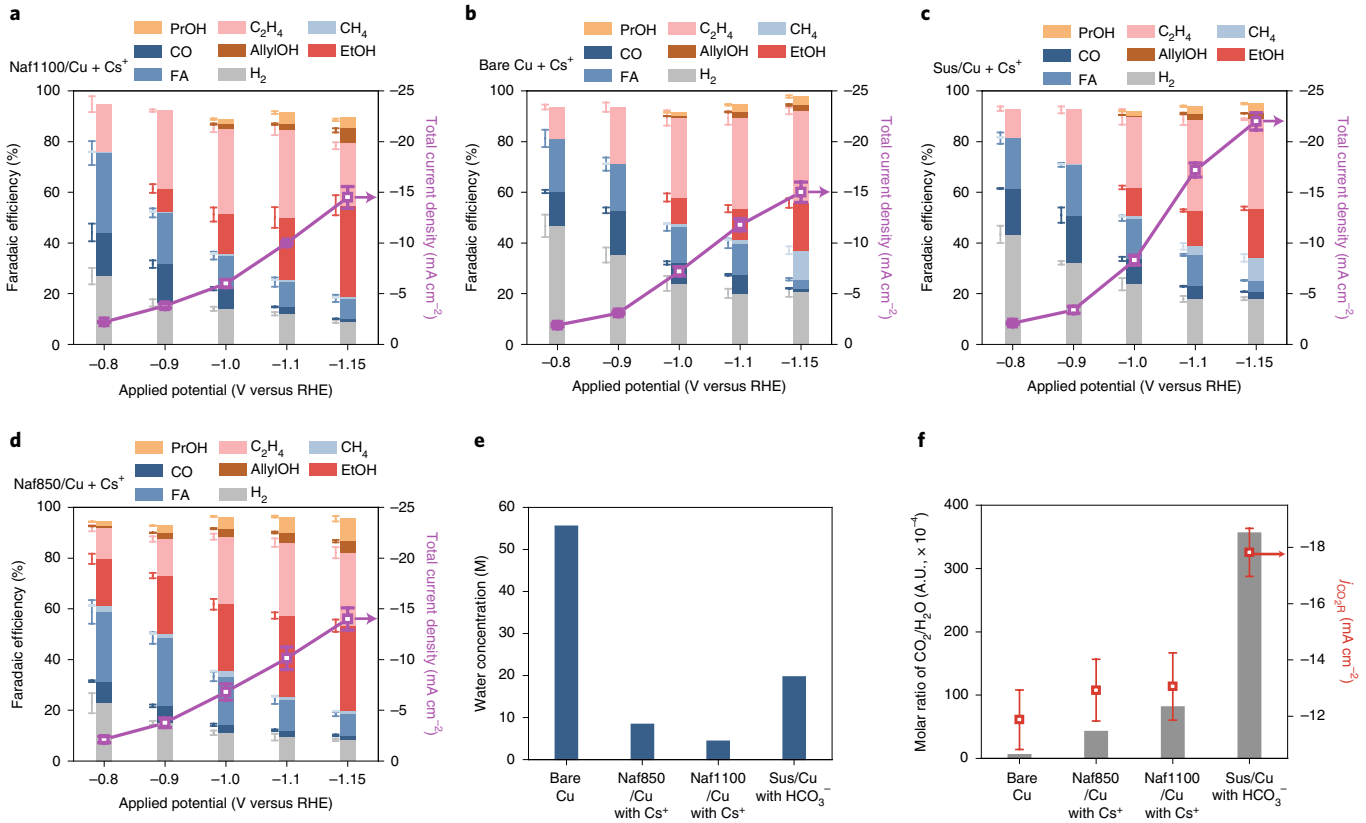

Fig. 2 | CO_2R using ionomer-coated Cu. a–d, Catalytic performance of CO_2R using Naf1100/Cu (**a**), bare Cu (**b**), Sus/Cu (**c**) and Naf850/Cu (**d**) in the presence of 0.1 M $CsHCO_3$ electrolyte. **e**, Measurement of water concentration for ionomer-coated Cu at 100% relative humidity; each sample was ion-exchanged using 0.1 M $CsHCO_3$ electrolyte before the measurement. **f**, Estimation of local CO_2/H_2O on the basis of measured water concentration in **e** and corresponding partial current densities at −1.15 V versus RHE (open symbols). In **a–d** and **f**, error bars indicate standard deviation among values from three repeated measurements.

is more likely to be related to modulation of the microenvironment near the Cu surface than to modifications of the surface, which would only be governed by the innermost ionomer layer. These phenomena are illustrated schematically in Fig. 5a–c.

This finding agrees well with the conclusions drawn from previous studies of CO_2R using Nafion-coated Cu, where changes to the Cu surface were not observed or inferred[21,27]. Additionally, as shown in Fig. 4b, when a Nafion layer was deposited on top of Cu or Sus/Cu, not only H_2 formation, but also C_1 formation relative to C_{2+} formation decreased considerably. However, although Sus/Cu exhibited a lower rate of H_2 formation and C_1 versus C_{2+} products compared with bare Cu, Sus/Naf850/Cu resulted in higher rates of C_1 formation than Naf850/Sus/Cu. These results demonstrate that the best chemical microenvironment for CO_2R on Cu is achieved when Nafion is placed at the outermost layer. As shown in Fig. 4c, for the case of Naf850/Sus/Cu, an ideal scenario of high local CO_2/H_2O ratio and greater OH^- accumulation due to Donnan exclusion is realized. Additionally, an outer layer of Nafion also hinders HCO_3^- transport from the bulk electrolyte to the reaction surface, thereby ameliorating its detrimental impact on pH and subsequent enhancement of C_1 over C_{2+} production (as shown in Fig. 5c). By contrast, for Sus/Naf850/Cu, accumulation of OH^- would only occur at the Cu/inner Nafion interface, providing a shorter pathway for OH^- transport and thus a lower pH at the Cu surface compared to Naf850/Sus/Cu. Additionally, when Sustainion is placed in the outermost layer, it is probably exchanged with a substantial concentration of HCO_3^-, which could negatively impact performance by buffering the increase in pH within the catalyst microenvironment[16].

This explanation is supported experimentally by observing reduced and enhanced hydrogen evolution reaction when acetonitrile is reduced electrochemically to ethylamine on Cu coated with Nafion and Sustainion, respectively. Whereas acetonitrile reduction is pH-insensitive, the selectivity for the hydrogen evolution reaction decreases with increasing pH[28] (Supplementary Fig. 11). Thus, the anion-exchange ionomer (AEI) enhances the local ratio of CO_2/H_2O due to its high CO_2 solubility (Fig. 5b), and the cation-exchange ionomer (CEI) increases the local pH by trapping CO_2R-generated OH^- and blocking the transport of buffering carbonate species into the catalyst microenvironment (Fig. 5c).

It is also important to make note of the similarities and differences between the bilayer thin-film environment and a bipolar membrane (BPM) CO_2 electrolyser, which has been of extensive interest due to its potential to mitigate parasitic carbonate cross-over[29–32]. Indeed, the Naf/Sus/Cu system is similar to a BPM operating in forward bias, in which the AEI is paired with the cathode, the CEI is paired with the anode and protons and hydroxides combine at the AEI–CEI interface to form water. The generation of water at the interface could potentially cause delamination at higher current densities. However, recent work has demonstrated that a well-matched pair of ionomers can achieve substantial adhesion and would not be as prone to delamination[33]. Therefore, for high current density applications, it will be necessary to properly identify a suitable pair of ionomers that will not delaminate at high current.

When invoking the analogous behaviour of the Sus/Naf/Cu system to a BPM in reverse bias, where the AEI is paired with the anode, the CEI is paired with the cathode and a catalyst placed at

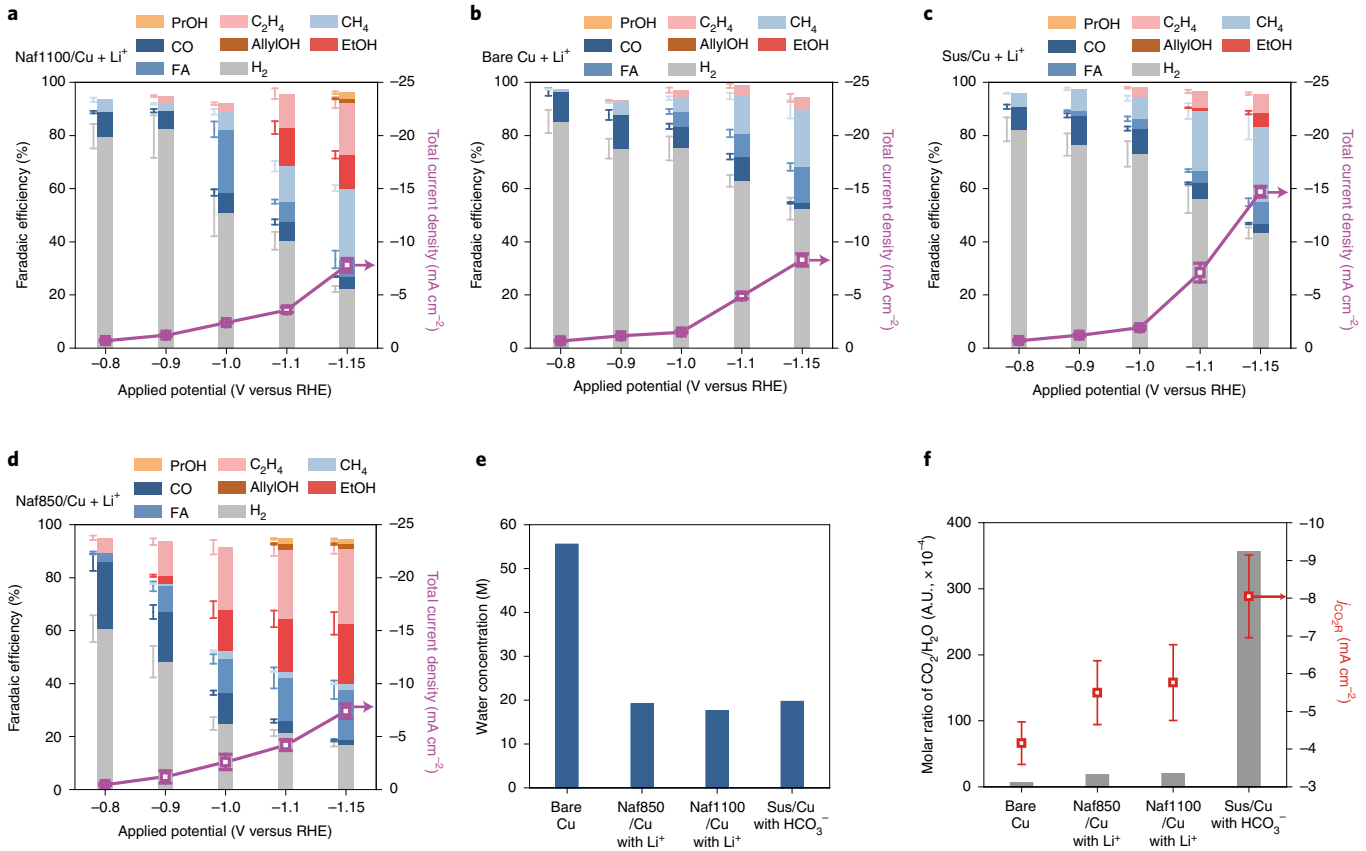

Fig. 3 | Effect of cation identity on CO_2R using ionomer-coated Cu. a–d, Catalytic performance of CO_2R using Naf1100/Cu (**a**), bare Cu (**b**), Sus/Cu (**c**) and Naf850/Cu (**d**) in the presence of 0.1 M $LiHCO_3$ electrolyte. **e**, Measurement of water concentration for ionomer-coated Cu at 100% relative humidity; each sample was ion-exchanged using 0.1 M $LiHCO_3$ electrolyte before the measurement. **f**, Estimation of local molar ratio between CO_2 and H_2O and corresponding partial current densities at −1.15 V versus RHE (open symbols). In **a**–**d** and **f**, error bars indicate standard deviation among values from three repeated measurements.

the AEI–CEI interface enables the dissociation of water into protons and hydroxides, a key distinction must be made. The Sus/Naf/Cu system employed in this study does not utilize a water dissociation catalyst, and, therefore, for the modest potentials applied here there is probably no water dissociation occurring at the AEI–CEI interface[34]. Previous studies have shown that when CO_2R occurs near a water dissociation catalyst, the reduction in pH due to the generation of protons from water dissociation leads to excessive H_2 generation on a Ag catalyst[23]. If there was noticeable water dissociation in the case of Sus/Naf/Cu, the pH reduction from water dissociation would lead to the selective generation of CH_4 and H_2. Because the major products in the case of Sus/Naf/Cu are still C_{2+} products, it is likely that water dissociation is not the primary driver of current in our system, marking a key difference between Sus/Naf/Cu and that of a reverse-bias BPM. This difference further emphasizes the fact that, while these systems are ostensibly similar, the different scale and application of the thin films when compared to those of a bulk BPM leads to drastically different microenvironments and may make traditional BPM issues less relevant.

The substantially improved performance demonstrated using the bilayer ionomer films described in this study raises questions regarding the interplay between ion transport and electrode kinetics within the ionomer films. These questions require the development of multiphysics, multiscale models to understand these new materials and how they alter the microenvironments near the electrode surface. Future work should also aim to understand the performance of bilayer catalyst coatings in higher current density applications, such as those achieved in membrane-electrode assembly or flow-cell devices for CO_2R. The concept of hydroxide trapping by Nafion has already been posed as an explanation for enhanced local pH observed in studies for CO_2R at high current densities[26,35]. The experiments reported for monopolar Nafion in flow cells provide confidence that the effects demonstrated here should be applicable to high current density operation. Additionally, there is immense potential to pair the Naf/Sus/Cu system with a bulk cation-exchange membrane to substantially inhibit parasitic carbonate cross-over, while also maintaining the high selectivity observed in the presented work.

Modification of the microenvironment by pulsed electrolysis

Recent studies have shown considerable enhancement in the FE for C_{2+} products relative to that of H_2, as well as an enhancement in TCD, when electrolysis is conducted with a square-waveform potential profile between −0.80 and −1.15 V versus RHE for 10 s each, compared to time-averaged static electrolysis at both potentials. These effects have been attributed to increased pH and CO_2 concentration within the dynamic microenvironment[7,15]. To examine whether this effect adds to that of the ionomer, pulsed CO_2 electrolysis was conducted with ionomer-coated Cu using the same voltage waveform. It is noted that cathodic potentials were chosen at much more negative potentials than the redox potential of Cu (0.42 V versus RHE) to avoid Cu surface modification. As shown in Fig. 6a and Supplementary Fig. 12, there was a clear compounding

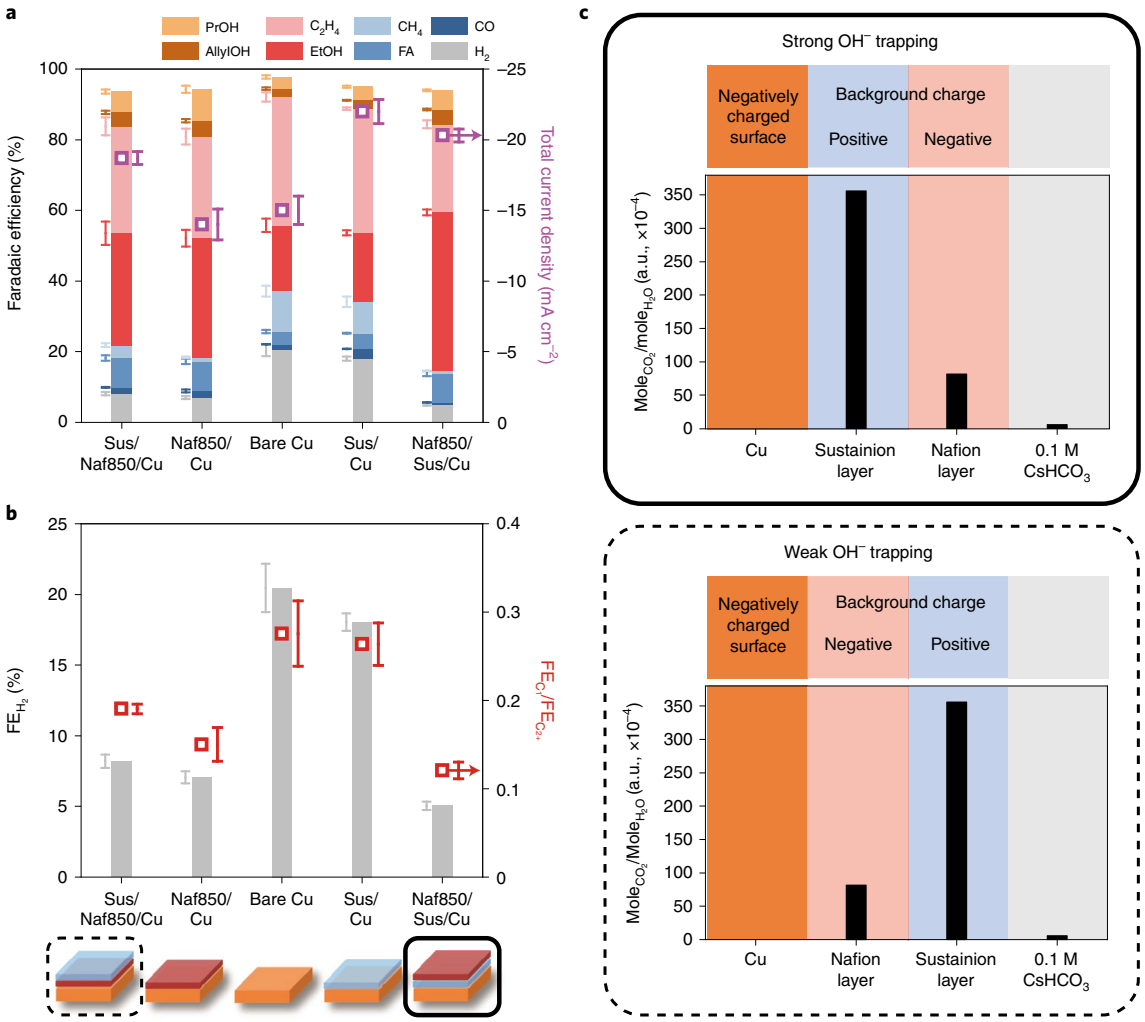

Fig. 4 | Effect of stacking ionomer layers. a, CO_2R performance at −1.15 V versus RHE using stacked ionomers on Cu in the presence of 0.1 M $CsHCO_3$ electrolyte. **b**, Trend in H_2, C_1 and C_{2+} formation for ionomer-coated Cu tested in **a**. It is noted that the ratio of FE for C_1 and that C_{2+} in the right axis of **b** is dimensionless. In **a** and **b**, error bars indicate standard deviation among values from three repeated measurements. **c**, Schematic illustration of Naf850/Sus/Cu (top) and Sus/Naf850/Cu (bottom) in terms of local CO_2/H_2O ratio (dimensionless) and spatial charge configuration. Areas shaded orange, blue, red and grey correspond to Cu, Sustainion, Nafion and electrolyte solution, respectively.

of effects between pulsed electrolysis and Naf850/Sus/Cu (Nafion as the outermost layer): the H_2 FE was suppressed below 4%, the C_{2+} FE was enhanced to 90% and the TCD increased to 12.1 mA cm^{-2}. On the other hand, there was a negative impact of pulsed electrolysis with Sus/Naf850/Cu (Sustainion as the outer layer): the H_2 FE increased to 20%, the C_{2+} FE decreased below 50% and the TCD remained unchanged. These results can be interpreted in terms of the effects of pulsing on the local pH and CO_2 concentration. When Nafion is in the outer layer, the increased current density and C_{2+} selectivity can be attributed to the higher CO_2/H_2O ratio in the inner Sustainion layer as well as the higher local pH due to OH^- trapping caused by the spatial charge distribution, both of which are enhanced by pulsed electrolysis (Fig. 4d). However, when Sustainion is in the outer layer, the local HCO_3^- concentration increases, thereby buffering the pH increase due to pulsing.

This hypothesis is supported by analysis of differential electrochemical mass spectrometry, which suggests that for all cases where Sustainion is on the outer layer the local pH rise on increasing the overpotential is not noticeable (Supplementary Fig. 13). Additionally, the hypothesis that an outer Sustainion layer enhances the local HCO_3^- concentration is further supported by enhancement of the CH_4 FE on pulsing with an outer Sustainion layer. We also note that recent studies have shown that CH_4 generation is enhanced selectively by pulsed electrolysis when the HCO_3^- concentration is increased[7,16]. Furthermore, CO_2R performance during pulsed electrolysis using Naf850/Sus/Cu could be optimized by varying the duration at each potential (Supplementary Figs. 14 and 15)[7]. As shown in Fig. 6b, the synergy between the effects of pulsed electrolysis and ionomer layers is even more prominent when viewed in terms of the partial current density. The partial current density for H_2 decreased considerably from −2.03 mA cm^{-2} (mean value, Supplementary Note 4) to −0.60 mA cm^{-2}, a 70% reduction. On the other hand, the partial current density for C_{2+} product formation increased substantially from −4.79 to −12 mA cm^{-2}, an improvement of 250%.

Conclusions

This work clearly demonstrates that the activity and selectivity of Cu for CO_2R can be tuned by tailoring the chemical microenvironment near the surface of a Cu CO_2R catalyst using different

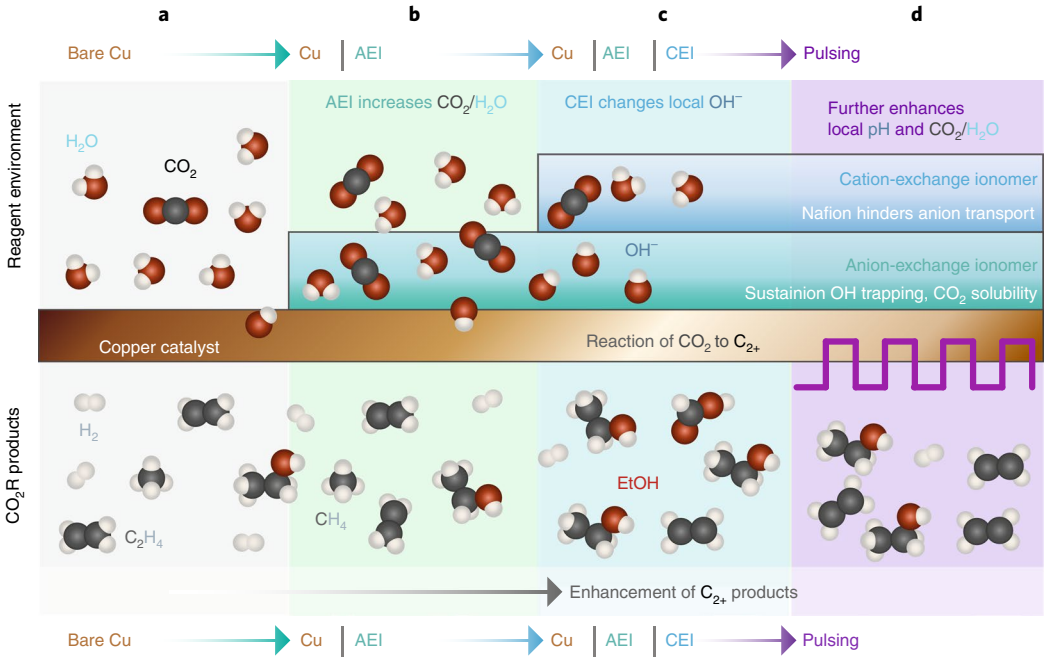

Fig. 5 | Schematic depiction of enhanced CO_2R using ionomers. a–d, Reference case where CO_2R takes place in the presence of a Cu catalyst (**a**), the relative improvement in performance with the addition of an AEI layer increasing local CO_2/H_2O ratio (**b**), with the addition of a CEI layer on AEI (**c**) thereby forming a bilayer local environment and modulating the local OH^- and with the pulsed electrolysis further enhancing the C_{2+} products (**d**). The changes in molecules and products (**a–d**) are depicted qualitatively on the basis of the experimental results but should not be taken as a direct representation.

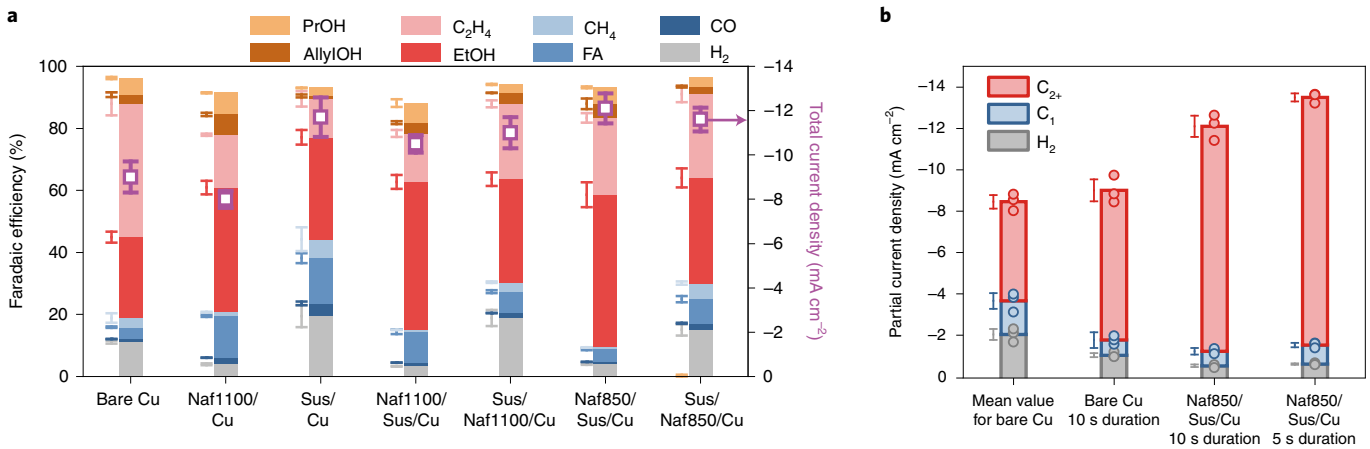

Fig. 6 | Synergy between microenvironment using ionomer layers and pulsed CO_2 electrolysis. a, Faradaic efficiencies of pulsed CO_2 electrolysis using various ionomer-coated Cu catalysts. Pulsed electrolysis was conducted using a square-wave potential pulse of 10 s duration at −1.15 and −0.8 V versus RHE for each potential. **b**, Partial current densities obtained under various conditions and configurations. In **a** and **b**, error bars indicate standard deviation among values from three repeated measurements.

anion- and cation-conducting ionomer layers (that is, bilayer thin films). We also show that the surface microenvironment can be further modified by pulsed electrolysis to achieve 90% C_{2+} FE and 4% H_2 FE. As discussed, the changes are achieved by strategic control of the pH and the local concentrations of H_2O and CO_2 near the surface of Cu, using ion screening and intrinsic ionomer properties: the anion-exchange ionomer exhibits increased CO_2 solubility, the cation-exchange ionomer increases the local pH by OH^- trapping and both layers impact the overall water concentration. As illustrated here for CO_2R and acetonitrile reduction, the rational design and implementation of composite ionomer layers are broadly applicable and directly translatable to other electrochemical syntheses, where low reactant solubility and complex pH dependencies govern product selectivity, thereby enabling selective synthetic pathways to a variety of products, such as C_4 oxygenates and hydrocarbon, azoxy-, azo-, amino-aromatics, adiponitrile and ammonia[28,36–39]. Additionally, while this work has only explored current densities of the order of 10 to 20 mA cm^{-2} due to mass transport limitations in aqueous phase CO_2 electrolysis, the fundamental knowledge gained here may be built on in future studies of vapour-fed CO_2 electrolysers (for example, membrane-electrode assemblies) operating at current densities approaching 1 A cm^{-2}. Future investigation of this

exciting class of catalyst coatings and their use in such electrolysers will also reveal whether the enhanced selectivity to C_{2+} products reported here can be extended to operation at higher current densities, and whether bilayer films can be used to reduce CO_2 cross-over.

Methods

Preparation of Cu electrodes. The working electrode was prepared by sputtering Cu onto a microporous (20 nm pore size) PTFE pervaporation membrane (Hangzhou Cobetter Filtration Equipment), which was used as the catalyst support for differential electrochemical mass spectroscopy analysis. Before sputtering of Cu, the membrane was rinsed consecutively with acetone (≥99.5%, VWR), methanol (≥99.8%, VWR) and Milli-Q water (18.2 MΩ cm) for 30 min each. Cu was sputtered onto the PTFE membrane using an AJA ATC Orion-5 magnetron sputtering system equipped with a Cu target (99.999%, Kurt J. Lesker) with a deposition rate of 1 Å s^{-1} to achieve a thickness of 400 nm.

Preparation of ionomer layer on Cu electrode. Commercial Nafion (Sigma-Aldrich, perfluorinated ion-exchange resin, 1,100 g mol^{-1} EW, 10 wt% dispersion in water), Nafion with lower EW (Chemours, 850 g mol^{-1} EW, 20 wt% dispersion in 20 wt% *n*-propanol aqueous solution) and Sustainion dispersions (Dioxide Materials, alkaline ionomer 5% in ethanol) were cast onto Cu/PTFE. Stock solutions were prepared by diluting the ionomer solution with isopropyl alcohol (Sigma-Aldrich, 99.9%). Prepared stock solutions were drop-cast onto Cu/PTFE with different amounts of ionomers to achieve 2, 6 and 18 $\mu g_{ionomer}$ cm^{-2} and then dried at room temperature for 1 h.

Electrochemical reduction of CO_2. CO_2R was carried out in a flow-through electrochemical cell[15] (Supplementary Fig. 16). The cell had three electrodes: the ionomer-coated Cu/PFTE, an Ag/AgCl (filled with 3.4 M KCl, Leak-Free, Innovative Instruments) reference electrode and a platinum gauze (99.995%, Sigma-Aldrich) counterelectrode. The cathodic and anodic chambers were separated by an anion membrane (Selemion AMV, AGC Engineering). The electrolyte was either a 0.05 M solution of Cs_2CO_3 (99.995%, Sigma-Aldrich) or a 0.05 M solution of Li_2CO_3 (99.995%, Sigma-Aldrich) prepared using Milli-Q water pretreated to remove metal impurities by contacting with a chelating agent solution (Chelex 100, Na form, Sigma-Aldrich) before use. Prepared electrolytes were saturated with a flow of CO_2 (20 sccm, 99.999%, Praxair) for 45 min in a gas-tight reservoir to turn into 0.1 M of $CsHCO_3$ or 0.1 M of $LiHCO_3$ and circulated by a peristaltic pump (FH100M, Thermo Scientific) at a rate of 80 ml min^{-1}. Electrochemistry was performed using a potentiostat (VSP-300, Biologic). An uncompensated resistance (R_u) was determined by both potentiostatic electrochemical impedance spectroscopy and the current interrupt method and was compensated to 85% using the potentiostat. All potentials were converted to the RHE scale as $E_{RHE} = E_{Ag/AgCl} + 0.197\ V + 0.0591 \times pH$. It should be noted that the Sustainion film cast on Cu was pretreated using chronoamperometry at −0.7 V versus RHE for 30 min before conducting the CO_2RR, to convert the Sustainion to its bicarbonate form, since the as-cast Sustainion layer was in its original chloride form, which exhibits poor conductivity, as shown in Supplementary Fig. 17.

Pulsed electrolysis was performed following protocols reported previously[15]. Briefly, a rectangular-wave potential pulse consisting of a period at −1.15 V versus RHE followed by a period at −0.8 V versus RHE was employed. Cathode potentials were chosen to be incapable of surface oxidation due to more negative potentials than the reduction potential of Cu_2O (0.4 V versus RHE).

Thin-film preparation for measurement of water content. To obtain different counterion forms of ionomers, as-received Nafion with 1,100 g mol_{eq}^{-1} EW, Nafion with 850 g mol_{eq}^{-1} EW and Sustainion ionomer dispersions were dialysed for two days in respective salt solutions (for Nafion: 0.1 M $LiHCO_3$ and $CsHCO_3$ to obtain Li^+ and Cs^+ counterions; for Sustainion: 1 M KOH and 1 M $KHCO_3$ to obtain OH^- and HCO_3^-) and then washed in pure water for one day to remove any residual. Thin films were prepared using ionomer dispersions after ion exchange. Ionomer solutions were diluted by the addition of *n*-propanol/H_2O (1:1 by weight) (Sigma-Aldrich) to obtain a nominal target film thickness of 30 nm. The diluted solutions were stirred overnight, sonicated for 60 min and filtered before being spin-cast. Prepared solutions were spun-cast on Cu substrates at 4,000 r.p.m. for 1 min (WS-650-23B model, Laurell) until a uniform film was fabricated. Following spin-casting, thin-film samples were rest for 60 min before the test.

Ionomer thin-film ellipsometry and water content. Ionomer film thickness was measured in situ under varying relative humidity (RH) using a J.A. Woollam alpha-SE RC2-XI spectroscopic ellipsometer and N_2 as the humidifying gas at a flow rate of 500 sccm for all set points. Before sample testing, samples were exposed to 60 min of 0% and 100% RH, respectively, for preconditioning[40,41]. A two-layer model was built to derive the thickness and optical properties of the polymer films on optically characterized substrates. This two-layer model accounts for Cu substrate (optical properties of bare Cu were pre-recorded before thin-film casting) and a Cauchy layer for ionomer thin film and resulted in optical constant and thickness fits of mean squared error $<4\times10^{-3}$. The changes in thickness and complex refractive index were calculated for films exposed to 0 to 100% RH with 10% intervals in an in-house-constructed environmental cell held at ambient temperature. The cell was made with non-polarizing fused silica windows to maximize the amount of light transmitted. Thin-film thickness at a given RH, L_{RH}, is the average thickness after the sample reaches equilibrium. The dry thickness (L_0) was taken after the sample reached equilibration at 0% RH. The change in swelling (ΔL) was used to calculate the film through-plane swelling fraction according to the following equation:

$$\text{Swelling fraction}\ (\%) = \Delta L/L_0 \tag{1}$$

Water content (λ) of ionomer thin films was calculated using:

$$\lambda = \frac{\text{Swelling fraction} \times \text{EW} \times \rho_{H_2O}}{\rho_{\text{ionomer}} \times M_{H_2O}} \tag{2}$$

where EW is the equivalent weight of ionomer dispersion, M_{H_2O} and ρ_{H_2O} are the molar mass and density of water and ρ_{ionomer} is the density of ionomer[42].

CO_2R product analysis. The products produced by electrochemical CO_2 reduction were analysed by gas and liquid chromatography. Gaseous products were separated from the electrolyte in a gas-tight reservoir and analysed by an online gas chromatograph (7890B, Agilent) equipped with a pulsed-discharge helium ionization detector, a Hayesep-Q capillary column (Agilent) and a ShinCarbon ST column (Restek). He (99.9999%, Praxair) was used as the carrier gas. The quantitative analysis was conducted using calibration curves obtained by series of NIST-traceable standard gas mixtures (100 to 8,000 ppm, Airgas). Liquid products collected in the catholyte reservoir over a period of 60 min were analysed using high-performance liquid chromatography (HPLC) (UltiMate 3000, Thermo Scientific) equipped with a refractive index detector and Aminex HPX 87-H columns (Bio-Rad). The HPLC signal for each product was also analysed quantitatively using calibration curves on the basis of a series of standard solutions in the range of concentration from 0.1 to 20 mM for each product. FE corresponding to product *i* was calculated as follows.

$$\text{FE}_i = \frac{n\text{FC}_i V}{I_{\text{total}}} \times 100\,\% \tag{3}$$

where *n* is the number of electrons transferred, *F* is Faraday's constant, C_i is the molar concentration of species *i*, *V* is the total volumetric flow rate and I_{total} is the measured total current. For observation of temporal evolution for each product, differential electrochemical mass spectroscopy was conducted, and each mass spectrum during CO_2RR was obtained using a mass spectrometer (HPR40, Hiden Analytical) connected to the differential electrochemical mass spectroscopy cell. The temporal resolution for the acquisition of mass spectrometry data was optimized to achieve a sampling time of <0.5 s, as reported previously[15].

Data availability

All data for this study are available in the Supplementary Information. Source data are provided with this paper.

Received: 10 May 2021; Accepted: 14 September 2021;
Published online: 28 October 2021

References

1. Nitopi, S. et al. Progress and perspectives of electrochemical CO_2 reduction on copper in aqueous electrolyte. *Chem. Rev.* **119**, 7610–7672 (2019).
2. Verma, S. et al. Model for defining technoeconomic benchmarks in the electroreduction of CO_2. *ChemSusChem* **9**, 1972–1979 (2016).
3. Whipple, D. T. & Kenis, P. J. A. Prospects of CO_2 utilization via direct heterogeneous electrochemical reduction. *J. Phys. Chem. Lett.* **1**, 3451–3458 (2010).
4. Ebaid, M. et al. Production of C_2/C_3 oxygenates from planar copper nitride-derived mesoporous copper via electrochemical reduction of CO_2. *Chem. Mater.* **32**, 3304–3311 (2020).
5. Huang, Y., Chen, Y., Cheng, T., Wang, L.-W. & Goddard, W. A. Identification of the selective sites for electrochemical reduction of CO to C_{2+} products on copper nanoparticles by combining reactive force fields, density functional theory, and machine learning. *ACS Energy Lett.* **3**, 2983–2988 (2018).
6. Jiang, K. et al. Effects of surface roughness on the electrochemical reduction of CO_2 over Cu. *ACS Energy Lett.* **5**, 1206–1214 (2020).
7. Bui, J. C., Kim, C., Weber, A. Z. & Bell, A. T. Dynamic boundary layer simulation of pulsed CO_2 electrolysis on a copper catalyst. *ACS Energy Lett.* **6**, 1181–1188 (2021).
8. Liu, X. et al. pH effects on the electrochemical reduction of $CO_{(2)}$ towards C_2 products on stepped copper. *Nat. Commun.* **10**, 32 (2019).
9. Wang, L. et al. Electrochemical carbon monoxide reduction on polycrystalline copper: effects of potential, pressure, and pH on selectivity toward multicarbon and oxygenated products. *ACS Catal.* **8**, 7445–7454 (2018).

10. Resasco, J. et al. Promoter effects of alkali metal cations on the electrochemical reduction of carbon dioxide. *J. Am. Chem. Soc.* **139**, 11277–11287 (2017).
11. Ringe, S. et al. Understanding cation effects in electrochemical CO_2 reduction. *Energy Environ. Sci.* **12**, 3001–3014 (2019).
12. Clark, E. L. & Bell, A. T. in *Carbon Dioxide Electrochemistry: Homogeneous and Heterogeneous Catalysis* (eds Robert, M. et al.) Ch. 3 (Royal Society of Chemistry, 2020).
13. Resasco, J. & Bell, A. T. Electrocatalytic CO_2 reduction to fuels: progress and opportunities. *Trends Chem.* **2**, 825–836 (2020).
14. Singh, M. R., Clark, E. L. & Bell, A. T. Effects of electrolyte, catalyst, and membrane composition and operating conditions on the performance of solar-driven electrochemical reduction of carbon dioxide. *Phys. Chem. Chem. Phys.* **17**, 18924–18936 (2015).
15. Kim, C., Weng, L.-C. & Bell, A. T. Impact of pulsed electrochemical reduction of CO_2 on the formation of C_{2+} products over Cu. *ACS Catal.* **10**, 12403–12413 (2020).
16. Kimura, K. W. et al. Selective electrochemical CO_2 reduction during pulsed potential stems from dynamic interface. *ACS Catal.* **10**, 8632–8639 (2020).
17. Wakerley, D. et al. Bio-inspired hydrophobicity promotes CO_2 reduction on a Cu surface. *Nat. Mater.* **18**, 1222–1227 (2019).
18. Wei, X. et al. Highly selective reduction of CO_2 to C_{2+} hydrocarbons at copper/polyaniline interfaces. *ACS Catal.* **10**, 4103–4111 (2020).
19. Zhong, S. et al. Efficient electrochemical transformation of CO_2 to C_2/C_3 chemicals on benzimidazole-functionalized copper surfaces. *Chem. Commun.* **54**, 11324–11327 (2018).
20. Aeshala, L. M., Uppaluri, R. & Verma, A. Electrochemical conversion of CO_2 to fuels: tuning of the reaction zone using suitable functional groups in a solid polymer electrolyte. *Phys. Chem. Chem. Phys.* **16**, 17588–17594 (2014).
21. García de Arquer, F. P. et al. CO_2 electrolysis to multicarbon products at activities greater than 1 A cm^{-2}. *Science* **367**, 661–666 (2020).
22. Gupta, K., Bersani, M. & Darr, J. A. Highly efficient electro-reduction of CO_2 to formic acid by nano-copper. *J. Mater. Chem. A* **4**, 13786–13794 (2016).
23. Yan, Z., Hitt, J. L., Zeng, Z., Hickner, M. A. & Mallouk, T. E. Improving the efficiency of CO_2 electrolysis by using a bipolar membrane with a weak-acid cation exchange layer. *Nat. Chem.* **13**, 33–40 (2021).
24. Sadeghpour, M., Yusoff, R. & Aroua, M. K. Polymeric ionic liquids (PILs) for CO_2 capture. *Rev. Chem. Eng.* **33**, 183–200 (2017).
25. Vermaas, D. A., Wiegman, S., Nagaki, T. & Smith, W. A. Ion transport mechanisms in bipolar membranes for (photo)electrochemical water splitting. *Sustain. Energy Fuels* **2**, 2006–2015 (2018).
26. Lees, E. W. et al. Linking gas diffusion electrode composition to CO_2 reduction in a flow cell. *J. Mater. Chem. A* **8**, 19493–19501 (2020).
27. Wang, J. et al. Selective CO_2 electrochemical reduction enabled by a tricomponent copolymer modifier on a copper surface. *J. Am. Chem. Soc.* **143**, 2857–2865 (2021).
28. Xia, R. et al. Electrochemical reduction of acetonitrile to ethylamine. *Nat. Commun.* **12**, 1949 (2021).
29. Pătru, A., Binninger, T., Pribyl, B. & Schmidt, T. J. Design principles of bipolar electrochemical co-electrolysis cells for efficient reduction of carbon dioxide from gas phase at low temperature. *J. Electrochem. Soc.* **166**, F34–F43 (2019).
30. Rabinowitz, J. A. & Kanan, M. W. The future of low-temperature carbon dioxide electrolysis depends on solving one basic problem. *Nat. Commun.* **11**, 5231 (2020).
31. S. H. Sichao Ma, et al. Electrolyzer and method of use. US patent 20200220185A1 (2020).
32. Blommaert, M. A. et al. Orientation of a bipolar membrane determines the dominant ion and carbonic species transport in membrane electrode assemblies for CO_2 reduction. *J. Mater. Chem. A* **9**, 11179–11186 (2021).
33. Mayerhöfer, B. et al. On the effect of anion exchange ionomer binders in bipolar electrode membrane interface water electrolysis. *J. Mater. Chem. A* **9**, 14285–14295 (2021).
34. Bui, J. C., Digdaya, I., Xiang, C., Bell, A. T. & Weber, A. Z. Understanding multi-ion transport mechanisms in bipolar membranes. *ACS Appl. Mater. Interfaces* **12**, 52509–52526 (2020).
35. Huang, J. E. et al. CO_2 electrolysis to multicarbon products in strong acid. *Science* **372**, 1074–1078 (2021).
36. Blanco, D. E., Lee, B. & Modestino, M. A. Optimizing organic electrosynthesis through controlled voltage dosing and artificial intelligence. *Proc. Natl Acad. Sci. USA* **116**, 17683–17689 (2019).
37. Chong, X., Liu, C., Huang, Y., Huang, C. & Zhang, B. Potential-tuned selective electrosynthesis of azoxy-, azo- and amino-aromatics over a CoP nanosheet cathode. *Natl Sci. Rev.* **7**, 285–295 (2019).
38. Barton, Z. J. et al. Electrochemical reduction selectivity of crotonaldehyde on copper. *J. Appl. Electrochem.* **51**, 5–17 (2021).
39. Ren, Y. et al. Strategies to suppress hydrogen evolution for highly selective electrocatalytic nitrogen reduction: challenges and perspectives. *Energy Environ. Sci.* **14**, 1176–1193 (2021).
40. Kusoglu, A., Dursch, T. J. & Weber, A. Z. Nanostructure/swelling relationships of bulk and thin-film PFSA ionomers. *Adv. Funct. Mater.* **26**, 4961–4975 (2016).
41. Tesfaye, M., Kushner, D. I. & Kusoglu, A. Interplay between swelling kinetics and nanostructure in perfluorosulfonic acid thin-films: role of hygrothermal aging. *ACS Appl. Polym. Mater.* **1**, 631–635 (2019).
42. Gierke, T. D., Munn, G. E. & Wilson, F. C. The morphology in Nafion perfluorinated membrane products, as determined by wide- and small-angle X-ray studies. *J. Polym. Sci. Polym. Phys. Ed.* **19**, 1687–1704 (1981).
43. Shi, S., Weber, A. Z. & Kusoglu, A. Structure-transport relationship of perfluorosulfonic-acid membranes in different cationic forms. *Electrochim. Acta* **220**, 517–528 (2016).
44. Zheng, Y. et al. Water uptake study of anion exchange membranes. *Macromolecules* **51**, 3264–3278 (2018).
45. Ren, X., Myles, T. D., Grew, K. N. & Chiu, W. K. S. Carbon dioxide transport in Nafion 1100 EW membrane and in a direct methanol fuel cell. *J. Electrochem. Soc.* **162**, F1221–F1230 (2015).
46. Zeebe, R. E. On the molecular diffusion coefficients of dissolved CO_2,HCO_3^-, and CO_3^{2-} and their dependence on isotopic mass. *Geochim. Cosmochim. Acta* **75**, 2483–2498 (2011).
47. Crothers, A. R., Darling, R. M., Kusoglu, A., Radke, C. J. & Weber, A. Z. Theory of multicomponent phenomena in cation-exchange membranes: part II. Transport model and validation. *J. Electrochem. Soc.* **167**, 013548 (2020).
48. Liu, Z., Yang, H., Kutz, R. & Masel, R. I. CO_2. Electrolysis to CO and O_2 at high selectivity, stability and efficiency using sustainion membranes. *J. Electrochem. Soc.* **165**, J3371–J3377 (2018).

Acknowledgements

This work was supported by the Joint Center for Artificial Photosynthesis, a DOE Energy Innovation Hub, supported through the Office of Science of the US Department of Energy under award no. DE-SC0004993 and Liquid Sunlight Alliance, which is supported by the US Department of Energy, Office of Science, Office of Basic Energy Sciences, Fuels from Sunlight Hub under award no. DE-SC0021266.

Author contributions

C.K. performed catalyst preparation, electrochemical experiments, characterizations and data interpretation. J.C.B. performed data interpretation and theoretical calculations. X.L. performed sample preparation and measurement for water uptake on ionomer film. J.K.C. performed X-ray photoemission spectroscopy analysis of ionomer-coated Cu. A.T.B., A.Z.W. and A.K. supervised the project. All authors discussed the results and participated in the preparation of the manuscript.

Competing interests

The authors declare no competing interests.

Additional information

Supplementary information The online version contains supplementary material available at https://doi.org/10.1038/s41560-021-00920-8.

Correspondence and requests for materials should be addressed to Alexis T. Bell.

Peer review information *Nature Energy* thanks Feng Jiao and the other, anonymous, reviewers for their contribution to the peer review of this work.

Reprints and permissions information is available at www.nature.com/reprints.

Publisher's note Springer Nature remains neutral with regard to jurisdictional claims in published maps and institutional affiliations.